

## PT-symmetry management in oligomer systems

This content has been downloaded from IOPscience. Please scroll down to see the full text.

2013 J. Phys. A: Math. Theor. 46 485101

(<http://iopscience.iop.org/1751-8121/46/48/485101>)

View [the table of contents for this issue](#), or go to the [journal homepage](#) for more

### Download details:

This content was downloaded by: lambdau

IP Address: 150.214.144.158

This content was downloaded on 20/11/2013 at 08:49

Please note that [terms and conditions apply](#).

# PT-symmetry management in oligomer systems

R L Horne<sup>1</sup>, J Cuevas<sup>2</sup>, P G Kevrekidis<sup>3</sup>, N Whitaker<sup>3</sup>,  
F Kh Abdullaev<sup>4,5</sup> and D J Frantzeskakis<sup>6</sup>

<sup>1</sup> Department of Mathematics, Morehouse College, Atlanta, GA 30314, USA

<sup>2</sup> Grupo de Física No Lineal, Departamento de Física Aplicada I, Universidad de Sevilla, Escuela Politécnica Superior, C/ Virgen de África, 7, E-41011 Sevilla, Spain

<sup>3</sup> Department of Mathematics and Statistics, University of Massachusetts, Amherst, MA 01003-4515, USA

<sup>4</sup> Instituto de Física Teórica, Universidade Estadual Paulista, 01140-070, São Paulo, São Paulo, Brazil

<sup>5</sup> Department of Physics, Faculty of Science, International Islamic University of Malaysia, PO Box 141, 25710 Kuantan, Malaysia

<sup>6</sup> Department of Physics, University of Athens, Panepistimiopolis, Zografos, GR-15784 Athens, Greece

E-mail: [rhorne@morehouse.edu](mailto:rhorne@morehouse.edu), [jcuevas@us.es](mailto:jcuevas@us.es), [kevrekid@gmail.com](mailto:kevrekid@gmail.com) and [whitaker@math.umass.edu](mailto:whitaker@math.umass.edu)

Received 16 August 2013, in final form 19 October 2013

Published 19 November 2013

Online at [stacks.iop.org/JPhysA/46/485101](http://stacks.iop.org/JPhysA/46/485101)

## Abstract

We study the effects of management of the PT-symmetric part of the potential within the setting of Schrödinger dimer and trimer oligomer systems. This is done by rapidly modulating in time the gain/loss profile. This gives rise to a number of interesting properties of the system, which are explored at the level of an averaged equation approach. Remarkably, this rapid modulation provides for a controllable *expansion* of the region of exact PT-symmetry, depending on the strength and frequency of the imposed modulation. The resulting averaged models are analysed theoretically and their exact stationary solutions are translated into time-periodic solutions through the averaging reduction. These are, in turn, compared with the exact periodic solutions of the full non-autonomous PT-symmetry managed problem and very good agreement is found between the two.

PACS numbers: 63.20.Pw, 63.20.Ry

(Some figures may appear in colour only in the online journal)

## 1. Introduction

It has been about a decade and a half since the radical and highly innovative proposal of C Bender and his collaborators [1] regarding the potential physical relevance of Hamiltonians respecting parity (P) and time-reversal (T) symmetries. While earlier work was focused on an implicit postulate of solely self-adjoint Hamiltonian operators, this proposal suggested that

these fundamental symmetries may allow for a real operator spectrum within a certain regime of parameters which is regarded as the regime of exact PT-symmetry. On the other hand, beyond a critical parametric strength, the relevant operators may acquire a spectrum encompassing imaginary or even genuinely complex eigenvalues, in which case, we are referring (at the linear level) to the regime of broken PT-phase.

These notions were intensely studied at the quantum mechanical level, chiefly as theoretical constructs. Yet, it was the fundamental realization that optics can enable such ‘open’ systems featuring gain and loss, both at the theoretical [2–5] and even at the experimental [6, 7] level, that propelled this activity into a significant array of new directions, including the possibility of the interplay of nonlinearity with PT-symmetry. In this optical context, the well-known connection of the Maxwell equations with the Schrödinger equation was utilized, and Hamiltonians of the form  $H = -(1/2)\Delta + V(x)$  were considered at the linear level with the PT-symmetry necessitating that the potential satisfies the condition  $V(x) = V^*(-x)$ . Yet another physical context where such systems have been experimentally ‘engineered’ recently is that of electronic circuits; see the work of [8] and also the review of [9]. In parallel to the recent experimental developments (including also mechanical systems [10] and even whispering-gallery microcavities [11]), numerous theoretical groups have explored various features of both linear PT-symmetric potentials [12–36] and even of nonlinear ones such where a PT-symmetric type of gain/loss pattern appears in the nonlinear term [37–40].

Our aim in the present work is to combine this highly active research theme of PT-symmetry with another topic of considerable recent interest in the physics of optical and also atomic systems, namely that of ‘management’; see, e.g., [41, 42] for recent reviews. Originally, the latter field had a significant impact at the level of providing for robust soliton propagation in suitable regimes of the so-called dispersion/nonlinearity management. More recently, as the above references indicate, the possibility (in both nonlinear optics and atomic physics) of periodic—or other—variation also of the nonlinearity has become a tool of significant value and has enabled to overcome a number of limitations including e.g. the potential of catastrophic collapse of bright solitary waves in higher dimensions. In the PT-symmetric setting, the closest example to what we envision here was proposed in the context of models featuring bright solitons [43, 44] (hence encompassing a transverse spatial dimension rather than exploring ordinary differential equations for few sites, as in the cases considered herein). In that context, concurrent management of the gain *and* of the linear coupling was utilized as a method of stabilization of coupled bright solitary waves between the field bearing gain and the one featuring loss. This was found to make the solitary waves robust attractors of the dynamics. Here, we instead chiefly consider a temporal modulation of (just the linear in our case<sup>7</sup>) gain and loss of few node configurations (rather than continuum media). While it is also possible to modulate the linear coupling between the nodes, we will only briefly touch upon this possibility towards the end of our exposition. We should point out that our case is quite different from that of [43, 44], where the concurrent presence and identical form of the coupling and gain/loss management is critical for the form of the solutions and, thus, of the obtained stabilization results. Admittedly, in the optical setting, and over the propagation distance, the type of variation proposed herein may be harder to achieve. Nevertheless, in an electronic setting where the properties of gain can be temporally controlled by relevant switching devices, such a realization may be deemed as more feasible. Our argument herein is that it is also very worthwhile to consider this problem from the point of view of its implications.

<sup>7</sup> It is entirely straightforward to envision a modulation of the nonlinear potential too, but this will be deferred as a separate topic for future study.

In particular, in what follows, we illustrate that in the case of a rapid modulation (‘strong’ management [41, 42]), it is possible to understand the non-autonomous PT-symmetric system by considering its effective averaged form. We showcase this type of averaging in the case of PT-symmetric oligomers, previously explored in a number of works (see e.g. [12, 18, 28, 29, 35, 36, 40], among others). We examine, more specifically, the case of dimers and trimers [45] which are the most tractable (also analytically) among the relevant configurations. Our findings suggest that there are interesting features that arise in the averaged models which are, in turn, found to be confirmed by the original non-autonomous ones. For instance, in the case of the dimer, the averaged effective model develops an effective linear coupling (and nonlinear self-interaction) coefficient, which has a dramatic implication in controllably expanding the region of the exact PT-symmetric phase, as a function of the strength and frequency of the associated modulation. Our analysis clearly illustrates how this is a direct consequence of the averaging process, and the properties of the periodic solutions are reconstructed on the basis of the averaging and are favourably compared to the observations of the time-periodic solutions of the original non-autonomous system.

Our presentation is structured as follows. In section 2, we systematically develop the averaging procedure both for the dimer and for the trimer; the generalization to more sites will then be evident. In section 3, we provide some general insight on the existence and stability of solutions in these effective averaged systems. In section 4, we corroborate these results with numerical simulations of the full non-autonomous dimer/trimer systems, finding very good agreement between the two. Finally, in section 5, we summarize our conclusions and comment on some interesting directions for potential future work.

## 2. The averaged equations for the PT-symmetric dimer and trimer models

### 2.1. DNLS PT-symmetric dimer model

We start by considering the DNLS dimer model with a rapidly-varying gain/loss term of the form:

$$\begin{aligned} i \frac{du}{dt} &= \kappa v + |u|^2 u + i\gamma_0 u + \frac{i}{\epsilon} \gamma_1(t/\epsilon) u, \\ i \frac{dv}{dt} &= \kappa u + |v|^2 v - i\gamma_0 v - \frac{i}{\epsilon} \gamma_1(t/\epsilon) v, \end{aligned} \quad (1)$$

where  $t$  is the evolution variable,  $\epsilon$  is a small parameter,  $\gamma_0$  represents the linear gain and loss strength and  $\gamma_1(t/\epsilon)$  is the rapidly-varying gain/loss profile that will be central to our considerations herein. We now apply a multiple scale analysis to equation (1) in order to derive an averaged equation for our problem. First, we define the new variables  $\tau = t/\epsilon$  (fast scale) and  $T = t$  (slow scale), and introduce the transformations

$$u(t) = U(T, \tau) \exp[\Gamma(\tau)], \quad v(t) = V(T, \tau) \exp[-\Gamma(\tau)], \quad (2)$$

where  $\Gamma(\tau) = \int_0^\tau \gamma_1(\tau') d\tau'$ . This way, we cast equations (1) into the following form:

$$\begin{aligned} \frac{i}{\epsilon} \frac{\partial U}{\partial \tau} + i \frac{\partial U}{\partial T} &= \kappa \exp[-2\Gamma(\tau)] V + \exp[2\Gamma(\tau)] |U|^2 U + i\gamma_0 U, \\ \frac{i}{\epsilon} \frac{\partial V}{\partial \tau} + i \frac{\partial V}{\partial T} &= \kappa \exp[2\Gamma(\tau)] U + \exp[-2\Gamma(\tau)] |V|^2 V - i\gamma_0 V. \end{aligned} \quad (3)$$

Next, expanding the unknown fields  $U(T, \tau)$  and  $V(T, \tau)$  in powers of  $\epsilon$ , i.e.,

$$U(T, \tau) = \sum_{n=0}^{\infty} \epsilon^n U_n(T, \tau), \quad V(T, \tau) = \sum_{n=0}^{\infty} \epsilon^n V_n(T, \tau), \quad (4)$$

we derive from equations (3) the following results.

At the leading-order of approximation, i.e., at  $\mathcal{O}(1/\epsilon)$ , we obtain the equations  $i\partial U_0/\partial\tau = 0$  and  $i\partial V_0/\partial\tau = 0$ , which suggest that the fields  $U_0$  and  $V_0$  depend only on the slow time scale  $T$ , i.e.,

$$U_0(T, \tau) = \tilde{U}_0(T), \quad V_0(T, \tau) = \tilde{V}_0(T). \quad (5)$$

Additionally, at the order  $\mathcal{O}(1)$ , we obtain the following set of equations:

$$\begin{aligned} i\frac{\partial U_1}{\partial\tau} + i\frac{\partial U_0}{\partial T} &= \kappa \exp[-2\Gamma(\tau)]V_0 + \exp[2\Gamma(\tau)]|U_0|^2U_0 + i\gamma_0U_0, \\ i\frac{\partial V_1}{\partial\tau} + i\frac{\partial V_0}{\partial T} &= \kappa \exp[2\Gamma(\tau)]U_0 + \exp[-2\Gamma(\tau)]|V_0|^2V_0 - i\gamma_0V_0. \end{aligned} \quad (6)$$

Next, using the definition of the average of some function  $f(\tau)$  over a period  $T$  as  $\langle f(\tau) \rangle \equiv (1/T)\int_0^T f(\tau) d\tau$ , we average equations (6) over the period  $T_0$  of  $\gamma_1(\tau)$ , and obtain the equations:

$$\begin{aligned} \frac{i}{T_0} \int_0^{T_0} \frac{\partial U_1}{\partial\tau} d\tau &= \frac{1}{T_0} \int_0^{T_0} d\tau \left[ -i\frac{\partial \tilde{U}_0}{\partial T} + \kappa \exp[-2\Gamma(\tau)]\tilde{V}_0 + \exp[2\Gamma(\tau)]|\tilde{U}_0|^2\tilde{U}_0 + i\gamma_0\tilde{U}_0 \right] \\ \frac{i}{T_0} \int_0^{T_0} \frac{\partial V_1}{\partial\tau} d\tau &= \frac{1}{T_0} \int_0^{T_0} d\tau \left[ -i\frac{\partial \tilde{V}_0}{\partial T} + \kappa \exp[2\Gamma(\tau)]\tilde{U}_0 + \exp[-2\Gamma(\tau)]|\tilde{V}_0|^2\tilde{V}_0 - i\gamma_0\tilde{V}_0 \right], \end{aligned} \quad (7)$$

where we have also used the result in equations (5). The solvability condition for these equations is satisfied if derive the following set of averaged equations for  $\tilde{U}_0(T)$  and  $\tilde{V}_0(T)$ :

$$\begin{aligned} i\frac{\partial U_0}{\partial T} &= \kappa_1V_0 + g_1|U_0|^2U_0 + i\gamma_0U_0, \\ i\frac{\partial V_0}{\partial T} &= \kappa_2U_0 + g_2|V_0|^2V_0 - i\gamma_0V_0, \end{aligned} \quad (8)$$

where for convenience, we have dropped the tildes; the (constant) coefficients of the above system are given by:

$$\begin{aligned} \kappa_1 &\equiv \frac{\kappa}{T_0} \int_0^{T_0} \exp[-2\Gamma(\tau)] d\tau, \quad \kappa_2 \equiv \frac{\kappa}{T_0} \int_0^{T_0} \exp[2\Gamma(\tau)] d\tau, \\ g_1 &\equiv \frac{1}{T_0} \int_0^{T_0} \exp[2\Gamma(\tau)] d\tau = \frac{\kappa_2}{\kappa}, \quad g_2 \equiv \frac{1}{T_0} \int_0^{T_0} \exp[-2\Gamma(\tau)] d\tau = \frac{\kappa_1}{\kappa}, \end{aligned} \quad (9)$$

and it should be recalled that  $\Gamma(\tau) = \int_0^\tau \gamma_1(\tau') d\tau'$  for some choice of  $\gamma_1(\tau)$ . For example, the choice of  $\gamma_1(\tau) = \gamma_1 \cos(\tau)$  allows one to express  $\kappa_1$ ,  $\kappa_2$ ,  $g_1$  and  $g_2$  in terms of modified Bessel functions. In this case, the period  $T_0 = 2\pi$  and  $\gamma_1$  is a constant that controls the amplitude of the temporal modulation.

In the next section, we will follow the method employed above to derive an averaged set of equations for the DNLS PT-symmetric trimer model.

## 2.2. DNLS PT-symmetric trimer model

We now consider the following DNLS trimer model with a rapidly-varying gain/loss term:

$$\begin{aligned} i\frac{du}{dt} &= -\kappa v - |u|^2u - i\gamma_0u - \frac{i}{\epsilon}\gamma_1(t/\epsilon)u, \\ i\frac{dv}{dt} &= -\kappa(u+w) - |v|^2v, \\ i\frac{dw}{dt} &= -\kappa v - |w|^2w + i\gamma_0w + \frac{i}{\epsilon}\gamma_1(t/\epsilon)w, \end{aligned} \quad (10)$$

where we have used the same notation as in the case of the dimer. We again assume that the unknown fields depend on the fast and slow scales  $\tau$  and  $T$ , and can be expressed as:

$$u(t) = U(T, \tau) \exp[\Gamma(\tau)], \quad v(t) = V(T, \tau), \quad w(t) = W(T, \tau) \exp[-\Gamma(\tau)], \quad (11)$$

where  $\Gamma(\tau) = -\int_0^\tau \gamma_1(\tau') d\tau'$ , and  $U(T, \tau)$ ,  $V(T, \tau)$  and  $W(T, \tau)$  obey the following system:

$$\begin{aligned} \frac{i}{\epsilon} \frac{\partial U}{\partial \tau} + i \frac{\partial U}{\partial T} &= -\kappa \exp[-\Gamma(\tau)]V - \exp[2\Gamma(\tau)]|U|^2U - i\gamma_0U, \\ \frac{i}{\epsilon} \frac{\partial V}{\partial \tau} + i \frac{\partial V}{\partial T} &= -\kappa \exp[\Gamma(\tau)]U - \kappa \exp[-\Gamma(\tau)]W - |V|^2V, \\ \frac{i}{\epsilon} \frac{\partial W}{\partial \tau} + i \frac{\partial W}{\partial T} &= -\kappa \exp[\Gamma(\tau)]V - \exp[-2\Gamma(\tau)]|W|^2W + i\gamma_0W. \end{aligned} \quad (12)$$

Next, expanding, as before,  $U(T, \tau)$ ,  $V(T, \tau)$  and  $W(T, \tau)$  in powers of  $\epsilon$ , namely,

$$\begin{aligned} U(T, \tau) &= \sum_{n=0}^{\infty} \epsilon^n U_n(T, \tau), & V(T, \tau) &= \sum_{n=0}^{\infty} \epsilon^n V_n(T, \tau), \\ W(T, \tau) &= \sum_{n=0}^{\infty} \epsilon^n W_n(T, \tau), \end{aligned} \quad (13)$$

we obtain from equations (12) the following results.

First, at the order  $\mathcal{O}(1/\epsilon)$ , we obtain the equations  $i\partial U_0/\partial \tau = 0$ ,  $i\partial V_0/\partial \tau = 0$ , and  $i\partial W_0/\partial \tau = 0$ , which show that the fields  $U_0$ ,  $V_0$  and  $W_0$  depend only on the slow time scale  $T$ , i.e.,

$$U_0(T, \tau) = \tilde{U}_0(T), \quad V_0(T, \tau) = \tilde{V}_0(T), \quad W_0(T, \tau) = \tilde{W}_0(T). \quad (14)$$

Next, at the order  $\mathcal{O}(1)$ , we obtain the system:

$$\begin{aligned} i \frac{\partial U_1}{\partial \tau} + i \frac{\partial U_0}{\partial T} &= -\kappa \exp[-\Gamma(\tau)]V_0 - \exp[2\Gamma(\tau)]|U_0|^2U_0 - i\gamma_0U_0, \\ i \frac{\partial V_1}{\partial \tau} + i \frac{\partial V_0}{\partial T} &= -\kappa \exp[\Gamma(\tau)]U_0 - \kappa \exp[-\Gamma(\tau)]W_0 - |V_0|^2V_0, \\ i \frac{\partial W_1}{\partial \tau} + i \frac{\partial W_0}{\partial T} &= -\kappa \exp[\Gamma(\tau)]V_0 - \exp[-2\Gamma(\tau)]|W_0|^2W_0 + i\gamma_0W_0. \end{aligned} \quad (15)$$

Similarly to the case for the PT-symmetric dimer model, we average the above system over the period  $T_0$  of  $\gamma_1(\tau)$ . Then, employing the solvability conditions for the resulting system, i.e.,  $U_1(T, \tau)$ ,  $V_1(T, \tau)$  and  $W_1(T, \tau)$  are periodic in  $\tau$  with period  $T_0$ , we obtain the following set of averaged equations for  $\tilde{U}_0$ ,  $\tilde{V}_0$  and  $\tilde{W}_0$ :

$$\begin{aligned} i \frac{\partial \tilde{U}_0}{\partial T} &= -\tilde{\kappa}_1 \tilde{V}_0 - g_1 |\tilde{U}_0|^2 \tilde{U}_0 - i\gamma_0 \tilde{U}_0, \\ i \frac{\partial \tilde{V}_0}{\partial T} &= -\tilde{\kappa}_2 \tilde{U}_0 - \tilde{\kappa}_1 \tilde{W}_0 - |\tilde{V}_0|^2 \tilde{V}_0, \\ i \frac{\partial \tilde{W}_0}{\partial T} &= -\tilde{\kappa}_2 \tilde{V}_0 - g_2 |\tilde{W}_0|^2 \tilde{W}_0 + i\gamma_0 \tilde{W}_0, \end{aligned} \quad (16)$$

where as in the dimer case, tildes have been dropped; the coefficients of the above equations are given by:

$$\begin{aligned} \tilde{\kappa}_1 &\equiv \frac{\kappa}{T_0} \int_0^{T_0} \exp[-\Gamma(\tau)] d\tau, & \tilde{\kappa}_2 &\equiv \frac{\kappa}{T_0} \int_0^{T_0} \exp[\Gamma(\tau)] d\tau \\ g_1 &\equiv \frac{1}{T_0} \int_0^{T_0} \exp[2\Gamma(\tau)] d\tau, & g_2 &\equiv \frac{1}{T_0} \int_0^{T_0} \exp[-2\Gamma(\tau)] d\tau. \end{aligned} \quad (17)$$

Notice that  $g_1$  and  $g_2$  are given by expressions identical to those defined in the previous section. Additionally, we will again consider the case with  $\gamma_1(\tau) = \gamma_1 \cos(\tau)$  (with the constant  $\gamma_1$  being the modulation amplitude).

### 3. Analysis of the averaged systems

We will now find solutions of the averaged effective PT dimer and trimer models, and investigate their stability.

#### 3.1. DNLS PT-symmetric dimer model

In the average dimer case (see equation (8)), we seek stationary solutions in the form:

$$U_0(t) = a \exp(-iEt), \quad V_0(t) = b \exp(-iEt) \quad (18)$$

where amplitudes  $a, b$  are complex and frequency (or energy)  $E$  is real-valued. Moreover, using a polar decomposition for  $a$  and  $b$  of the form:

$$a = Ae^{i\phi_a}, \quad b = Be^{i\phi_b}, \quad (19)$$

we obtain the following set of real equations for  $A$  and  $B$ :

$$\begin{aligned} \kappa_1 B \sin(\Delta\phi) + \gamma_0 A &= 0, & -\kappa_2 A \sin(\Delta\phi) - \gamma_0 B &= 0 \\ EA = \kappa_1 B \cos(\Delta\phi) + g_1 A^3, & EB = \kappa_2 A \cos(\Delta\phi) + g_2 B^3, \end{aligned} \quad (20)$$

where  $\Delta\phi \equiv \phi_b - \phi_a$ . The compatibility condition of the equations containing  $\sin(\Delta\phi)$  yields:

$$A^2 = \frac{\kappa_1}{\kappa_2} B^2. \quad (21)$$

The above equation is then substituted into the compatibility condition of the equations containing  $\cos(\Delta\phi)$ , yielding the equation  $g_1 \kappa_1 = g_2 \kappa_2$ ; the latter is always satisfied, as seen by equation (9). Next, we use standard trigonometric identities to express  $A^2$  in terms of parameters  $\kappa_1, \kappa_2, \gamma_0$  and  $E$ ; this way, we obtain the algebraic equation  $(E - g_1 A^2)^2 + \gamma_0^2 = \kappa_1 \kappa_2$ , which leads to the result:

$$A^2 = \frac{E \mp \sqrt{\kappa_1 \kappa_2 - \gamma_0^2}}{g_1}, \quad (22)$$

with the  $\mp$  sign corresponding to two different solutions of the Hamiltonian limit. Obviously, in the case of  $g_1 > 0$ , the two solutions exist only when  $A^2$  is positive, and thus, respectively  $E > \sqrt{\kappa_1 \kappa_2 - \gamma_0^2}$  and  $E > -\sqrt{\kappa_1 \kappa_2 - \gamma_0^2}$  for the  $(-)$  and  $(+)$  signs, provided that  $\kappa_1 \kappa_2 - \gamma_0^2 > 0$ . In fact, the latter inequality defines the condition for being in the exact (and not in the broken) PT-symmetric phase i.e., the underlying linear (and even the fully nonlinear) problem of equations (8) has real eigenvalue solutions when the inequality is satisfied.

One can also examine the stability of the stationary solutions found for the PT-symmetric effective dimer case. Particularly, we consider the linearization ansatz on top of the stationary solutions of equation (8) to have the form:

$$U_0(t) = e^{-iEt} [a + p e^{\lambda t} + P e^{\lambda^* t}], \quad V_0(t) = e^{-iEt} [b + q e^{\lambda t} + Q e^{\lambda^* t}], \quad (23)$$

where the star denotes complex conjugate. Substituting the above ansatz into equation (8) and linearizing in  $p, P, q$  and  $Q$ , we obtain the eigenvalue problem:

$$\mathbf{A}\mathbf{X} = i\lambda\mathbf{X}, \quad (24)$$

where  $\mathbf{X} = (p, -P^*, q, -Q^*)^T$  and the  $4 \times 4$  matrix  $\mathbf{A}$  has elements  $a_{ij}$  given by:

$$\begin{aligned} a_{11} &= -E + 2g_1|a|^2 + i\gamma_0 & a_{12} &= -g_1a^2, & a_{13} &= \kappa_1, & a_{14} &= 0 \\ a_{21} &= g_1(a^*)^2, & a_{22} &= E - 2g_1|a|^2 + i\gamma_0, & a_{23} &= 0, & a_{24} &= -\kappa_1 \\ a_{31} &= \kappa_2, & a_{32} &= 0, & a_{33} &= -E + 2g_2|b|^2 - i\gamma_0, & a_{34} &= -g_2b^2 \\ a_{41} &= 0, & a_{42} &= -\kappa_2, & a_{43} &= g_2(b^*)^2, & a_{44} &= E - 2g_2|b|^2 - i\gamma_0. \end{aligned} \quad (25)$$

Upon substituting the parameters characterizing the solutions of the PT-symmetric dimer model into  $a_{ij}$ , and solving the eigenvalue problem (24), one can then find the eigenvalues  $\lambda$ , which determine the spectral stability of the corresponding nonlinear solutions: the existence of eigenvalues with positive real part,  $\lambda_r > 0$ , amounts to a dynamical instability of the relevant solution, while in the case where all the eigenvalues have  $\lambda_r \leq 0$ , the solution is linearly stable. We will offer more details on the specifics of the linearization analysis in the numerical section, for the particular choice of cosinusoidal dependence of  $\gamma$  on time considered herein.

### 3.2. DNLS PT-symmetric trimer model

First, we rewrite equations (16) in the following form:

$$\begin{aligned} i\frac{\partial U_0}{\partial t} &= k_1V_0 + g_1|U_0|^2U_0 + i\gamma_0U_0, \\ i\frac{\partial V_0}{\partial t} &= k_2U_0 + k_1W_0 + |V_0|^2V_0, \\ i\frac{\partial W_0}{\partial t} &= k_2V_0 + g_2|W_0|^2W_0 - i\gamma_0W_0 \end{aligned} \quad (26)$$

where the averaged coefficients  $k_1 \equiv -\tilde{\kappa}_1$ ,  $k_2 \equiv -\tilde{\kappa}_2$ ,  $g_1$  and  $g_2$  are given in equation (17). We again seek stationary solutions of the form:

$$U_0(t) = a \exp(-iEt), \quad V_0(t) = b \exp(-iEt), \quad W_0(t) = c \exp(-iEt) \quad (27)$$

where  $E$  is real-valued and the complex amplitudes  $a$ ,  $b$  and  $c$  are decomposed as:

$$a = Ae^{i\phi_a}, \quad b = Be^{i\phi_b}, \quad c = Ce^{i\phi_c}. \quad (28)$$

Substituting the above expressions into equations (26) we obtain the following system for  $A$ ,  $B$  and  $C$ :

$$\begin{aligned} k_1B \sin(\Delta\phi_1) + \gamma_0A &= 0, & k_2B \sin(\Delta\phi_2) - \gamma_0C &= 0, \\ EA = k_1B \cos(\Delta\phi_1) + g_1A^3, & EC = k_2B \cos(\Delta\phi_2) + g_2C^3, \\ EB = k_2A \cos(\Delta\phi_1) + k_1C \cos(\Delta\phi_2) + B^3, & \\ -k_2A \sin(\Delta\phi_1) - k_1C \sin(\Delta\phi_2) &= 0, \end{aligned} \quad (29)$$

where  $\Delta\phi_1 \equiv \phi_b - \phi_a$  and  $\Delta\phi_2 \equiv \phi_b - \phi_c$ . We determine non-trivial solutions for  $A$ ,  $B$  and  $C$  by solving the first four equations in equation (29) for  $\sin(\Delta\phi_1)$ ,  $\sin(\Delta\phi_2)$ ,  $\cos(\Delta\phi_1)$  and  $\cos(\Delta\phi_2)$ , and then plugging these results into the last two equations in equation (29). This way, we derive the following two consistency conditions:

$$k_1k_2B^4 - k_1k_2EB^2 + E(k_2^2A^2 + k_1^2C^2) - (k_2^2g_1A^4 + k_1^2g_2C^4) = 0, \quad \gamma_0(k_1^2C^2 - k_2^2A^2) = 0. \quad (30)$$

The second equation in (30) leads to a relation connecting  $C^2$  and  $A^2$ , namely  $C^2 = (k_2/k_1)^2A^2$ , which must be imposed to satisfy the first of equations (30). Using this relation, and the first



two sets of equations in (29), we find:

$$\begin{aligned} \cos(\Delta\phi_1) &= \frac{A(E - g_1A^2)}{k_1B}, & \cos(\Delta\phi_2) &= \pm \frac{A(E - g_2\left(\frac{k_2}{k_1}\right)^2A^2)}{k_1B}, \\ \sin(\Delta\phi_1) &= -\frac{\gamma_0A}{k_1B}, & \sin(\Delta\phi_2) &= \pm \frac{\gamma_0A}{k_1B}. \end{aligned} \quad (31)$$

To this end, we use trigonometric identities to finally connect  $A$  and  $B$  through the algebraic conditions:

$$\begin{aligned} g_1^2A^6 - 2Eg_1A^4 + (E^2 + \gamma_0^2)A^2 - k_1^2B^2 &= 0, \\ g_2^2\left(\frac{k_2}{k_1}\right)^4A^6 - 2Eg_2\left(\frac{k_2}{k_1}\right)^2A^4 + (E^2 + \gamma_0^2)A^2 - k_1^2B^2 &= 0. \end{aligned} \quad (32)$$

These equations are consistent (i.e., reduce to a single equation) if one requires  $g_1 = g_2(k_2/k_1)^2$ . Using this requirement, along with  $C^2 = (k_2/k_1)^2A^2$  and equation (30), we derive two equations that can be used to determine  $A$  and  $B$  explicitly:

$$\begin{aligned} k_1k_2B^4 - k_1k_2EB^2 + 2Ek_2^2A^2 - 2g_1k_2^2A^4 &= 0, \\ g_1^2A^6 - 2Eg_1A^4 + (E^2 + \gamma_0^2)A^2 - k_1^2B^2 &= 0, \end{aligned} \quad (33)$$

where  $C^2 = (k_2/k_1)^2A^2$  and  $g_1 = g_2(k_2/k_1)^2$ . One can then solve equations (33) for  $A$  and  $B$  in terms of parameters  $g_1, k_1, k_2, E, \gamma_0$  and  $g_2$ .

In a similar manner to the dimer case, once the relevant stationary states are obtained, one can examine the stability of the stationary solutions found for the PT-symmetric effective trimer case. We consider solutions of equations (26) of the form:

$$\begin{aligned} U_0(t) &= e^{-iEt}[a + pe^{\lambda t} + Pe^{\lambda^*t}], & V_0(t) &= e^{-iEt}[b + qe^{\lambda t} + Qe^{\lambda^*t}], \\ W_0(t) &= e^{-iEt}[c + re^{\lambda t} + Re^{\lambda^*t}]. \end{aligned} \quad (34)$$

Substituting this ansatz into equation (26) and linearizing in  $p, P, q, Q, r$  and  $R$ , we end up with the eigenvalue problem:

$$\mathbf{A}\mathbf{Y} = i\lambda\mathbf{Y}, \quad (35)$$

where  $\mathbf{Y} = (p, -P^*, q, -Q^*, r, -R^*)^T$  and the  $6 \times 6$  stability matrix  $\mathbf{A}$  has elements  $a_{ij}$  which are now given by:

$$\begin{aligned} a_{11} &= -E + 2g_1|a|^2 + i\gamma_0, & a_{12} &= -g_1a^2, & a_{13} &= k_1, & a_{14} &= 0, & a_{15} &= 0, & a_{16} &= 0, \\ a_{21} &= g_1(a^*)^2, & a_{22} &= E - 2g_1|a|^2 + i\gamma_0, & a_{23} &= 0, & a_{24} &= -k_1, & a_{25} &= 0, & a_{26} &= 0, \\ a_{31} &= k_2, & a_{32} &= 0, & a_{33} &= -E + 2|b|^2, & a_{34} &= -b^2, & a_{35} &= k_1, & a_{36} &= 0, \\ a_{41} &= 0, & a_{42} &= -k_2, & a_{43} &= (b^*)^2, & a_{44} &= E - 2|b|^2, & a_{45} &= 0, & a_{46} &= -k_1, \\ a_{51} &= 0, & a_{52} &= 0, & a_{53} &= k_2, & a_{54} &= 0, & a_{55} &= -E + 2g_2|c|^2 - i\gamma_0, & a_{56} &= -g_2c^2, \\ a_{61} &= 0, & a_{62} &= 0, & a_{63} &= 0, & a_{64} &= -k_2, & a_{65} &= g_2(c^*)^2, & a_{66} &= E - 2g_2|c|^2 - i\gamma_0. \end{aligned} \quad (36)$$

As before, substitution of the parameters of the solutions in  $a_{ij}$ , and solution of (35) will lead to the eigenvalues that determine the spectral stability of the corresponding nonlinear solutions. Once again, the details of the linear stability properties will be explored in the upcoming numerical section.

#### 4. Numerical results for the modulated system and comparison to the averaged models

We show below the results of the numerical analysis of the full non-autonomous system of equations (1) and (10) and compare them to those of the averaged equations derived above. In order to simplify the notation, we denote  $y \equiv \{u, v\}$  for the dimer and  $y \equiv \{u, v, w\}$  for the trimer. We seek solutions  $y(t)$  in the form

$$y(t) = \exp(-iEt)x(t), \quad (37)$$

with  $x(t)$  being a periodic orbit of period  $T_b = 2\pi/\omega$  that is found by means of a shooting method, i.e. by looking for fixed points of the map  $x(0) \rightarrow x(T_b)$ . The stability of the periodic orbit is obtained by means of a Floquet method, which identifies the relevant Floquet multipliers; see e.g. [46] for a relevant discussion and several application examples. In order to apply the Floquet method, a small perturbation  $\xi(t)$  is added to a given solution  $x(t)$ , and the stability properties of the solutions are given by the spectrum of the Floquet operator whose matrix representation is the *monodromy* matrix  $\mathcal{M}$ . The monodromy matrix eigenvalues  $\Lambda$  are dubbed as Floquet multipliers. This operator is real, which implies that the eigenvalues come in pairs  $\{\Lambda, \Lambda^*\}$ . In addition, there is always a pair of multipliers at 1 (corresponding to the so-called phase and growth modes).

In order to preserve the PT-symmetry of the system,  $\gamma_1(t)$  must be even in time. In that light, as indicated above, we have chosen

$$\gamma_1(t) = \gamma_1 \cos(\omega t), \quad (38)$$

i.e.,  $\epsilon \equiv 1/\omega$  and  $\tau = t/\epsilon = \omega t$  in equations (1) and (10); consequently, if the period of  $\gamma_1$  is  $T_0 = 2\pi$ , this implies that

$$\frac{1}{T_0} \int_0^{T_0} \exp[\pm\beta\Gamma(\tau)] d\tau = I_0(\beta\gamma_1), \quad (39)$$

with  $\beta$  being an arbitrary real number, and  $I_0$  being the zeroth-order modified Bessel function of the first kind. Given that  $I_0(x) = I_0(-x)$ , we can write  $\kappa_1 = \kappa_2 = \kappa' \equiv \kappa I_0(\beta_1\gamma_1)$ ,  $g_1 = g_2 = g' \equiv I_0(\beta_2\gamma_1)$ , with the values of  $\beta_1$  and  $\beta_2$  depending on the particular oligomer we are dealing with.

We have compared below the numerical results of the full non-autonomous problem with the predictions from the averaged system when the modulation amplitude is  $\gamma_1 = 1$  (results for other values of  $\gamma_1$  were also considered, and qualitatively similar conclusions were obtained). We have analysed a fast modulation  $\omega = 1000$  and a considerably slower one of  $\omega = 20$ . In the former case, the agreement is excellent, i.e., the curves from the non-autonomous and the averaged problem cannot be distinguished; for this reason, the results for that case will not be shown. Thus, below, we will restrict our numerical presentation to the slower modulated case of  $\omega = 20$ .

The quantities compared between the effective averaged solution properties and those of the non-autonomous system are the Floquet multipliers, which are related to the stability eigenvalues  $\lambda$  of the averaged system as:

$$\Lambda = \exp(2\pi\lambda/\omega), \quad (40)$$

and the averaged  $\ell^2$  norm (or average power) of the corresponding vector  $y$ , defined as

$$\langle N \rangle = \frac{1}{T_b} \int_0^{T_b} |y(t)|^2 dt. \quad (41)$$

Note that the predictions made for the averaged system are only able to obtain  $Y \equiv \{U, V\}$  or  $Y \equiv \{U, V, W\}$ , so the change of variables in (2) or (11) must be taken into account in order to find  $y(t)$ .

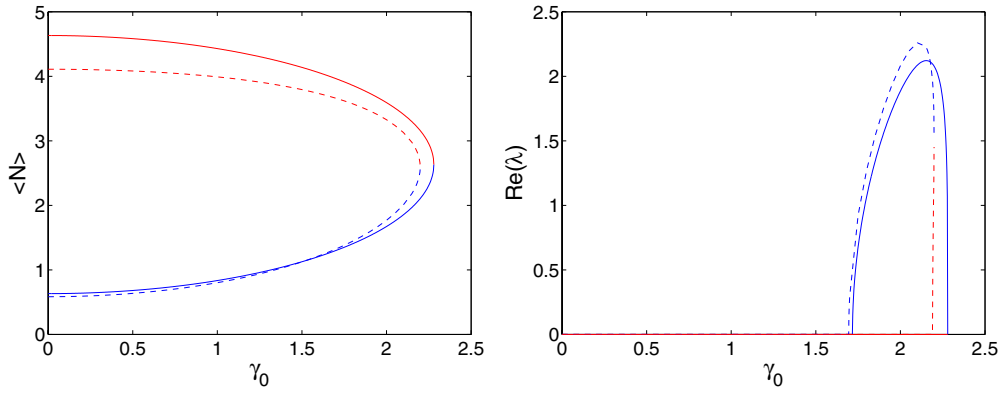


**Figure 1.** Averaged norm (left panel) and real part of the stability eigenvalues (right panel) for a dimer with  $\kappa = 1$ ,  $E = 3$  and  $\gamma_1 = 1$ ,  $\omega = 20$ . Solid (dashed) lines represent the values for the averaged (modulated) system, whereas blue (red) corresponds to the S (A) solution. The designation of S (symmetric) or A (anti-symmetric) corresponds to the  $\gamma_0 = 0$  Hamiltonian limit of the problem where  $\Delta\phi = 0$  or  $\pi$ , respectively.

#### 4.1. DNLS PT-symmetric dimer model

In this case,  $\kappa' = \kappa q$ , and  $g' = q$  with  $q = I_0(2\gamma_1)$ , and, consequently, (21) yields for the averaged system:

$$A^2 = B^2 = \frac{E \mp \sqrt{\kappa^2 q^2 - \gamma_0^2}}{q}, \quad (42)$$

with the  $\mp$  sign corresponding, respectively, to the symmetric (S) and anti-symmetric (A) solution (of the Hamiltonian limit). The symmetric or anti-symmetric character of the periodic orbit at the Hamiltonian limit can be easily deduced from (20), where the choice of  $\Delta\phi = 0$  (i.e. symmetric solution) implies a minus sign in (42) while the plus sign is obtained by using  $\Delta\phi = \pi$  (anti-symmetric solution). Consequently, from (42), it is clear that there is a saddle-center bifurcation at  $\gamma_0 = \kappa q$ . Above this value, the amplitudes become imaginary and the relevant analytical solutions of the effective system do not exist. This is precisely, the nonlinear analogue of the PT phase transition; note that the latter, especially in the case of the dimer, coincides with the linear PT phase transition. A remarkable feature that we observe in this context is that, since  $q > 1$ , the critical point for both the linear and the nonlinear PT-symmetry-breaking transition will be increased, hence the region of gain/loss parameters  $\gamma_0$  corresponding to an exact PT-symmetric phase will be expanded (possibly quite considerably and, in any case, controllably so) with respect to the unmodulated case.

Interestingly, in the case of the dimer, following the analysis of [18], the linear stability eigenvalues can be analytically found for the effective dimer as:

$$\lambda = \pm 2i \sqrt{2(\kappa^2 q^2 - \gamma_0^2) \mp E \sqrt{\kappa^2 q^2 - \gamma_0^2}}. \quad (43)$$

The numerical analysis of the modulated system is done by choosing  $\kappa = 1$  and  $E = 3$ . As explained above,  $\gamma_1 = 1$ , with  $\omega = 20$ , yielding  $q = I_0(2) \approx 2.2796$ . If  $E > q$ , the S and A solutions exist at  $\gamma_0 = 0$ .

Figure 1 shows both the averaged norm and the real part of the stability eigenvalues, together with the predicted values by the averaged equations. We can observe that the bifurcation designated as the nonlinear analogue of the PT-phase transition (leading to the

collision and disappearance of the—former—symmetric and anti-symmetric solutions of the  $\gamma_0 = 0$  limit) takes place only slightly earlier in the non-autonomous system (at  $\gamma_0 = 2.1989$ ). Regarding the stability, it is predicted in the averaged system that the S solution becomes unstable for  $\gamma_0 = \sqrt{\kappa^2 q^2 - E^2/4} \approx 1.7165$ ; in the modulated system, this bifurcation takes place around  $\gamma_0 = 1.6945$  (i.e., again at a very proximal value). Additionally, and quite interestingly, even the A solution may become unstable close to the transition point i.e, for  $\gamma_0 > 2.1899$ . This feature is not captured by the averaged equations but also only appears to be a very weak and hence not particularly significant effect physically. Note that the fact that both pairs of multipliers for the A and S solutions come in towards the bifurcation point from the unstable side has been observed recently in a PT-symmetric Klein–Gordon dimer [47].

Figure 2 shows the dynamical evolution of stable and unstable (A and S) solutions. The top panels illustrate a case example of stable oscillations for  $\gamma_0 = 1.5$ . Notice, however, that this value of the gain/loss parameter is already above the critical one in the absence of modulation, clearly showcasing the extension of the PT-symmetric regime due to the presence of the modulation. Here, the elements of both branches execute stable periodic motion. In the second row, for  $\gamma_0 = 2$ , the former anti-symmetric oscillation remains stable, but the former symmetric one is in its regime of instability, thus giving rise to a modulated form of growth, whereby the gain site grows indefinitely while the lossy site ultimately approaches a vanishing amplitude. The third row shows the evolution for  $\gamma_0 = 2.195$ , a value for which both A and S solutions are unstable. At the *modified* threshold (fourth row) of the PT-symmetry breaking, both branches are sensitive to perturbations and can give rise to growth of one node and decay of the other. This type of behaviour is also generically observed to be relevant for initial data beyond the PT-phase transition threshold, as is shown in the bottom row.

A comment would be useful here about the accuracy of the averaging method. Since in our averaging approach, we are capturing the effective correction to the dimer (and trimer) coefficients at  $O(1/\omega)$ , where  $\omega$  represents the frequency of the drive, it is expected that the error in our approximations will be growing according to  $O(1/\omega^2)$  i.e., the next term in the expansion. This is confirmed in figure 3, where the error in the approximation of the S and A branches of the dimer by our averaging is computed numerically as a function of  $\omega$ . The best fit slope of the relevant log–log plot is  $\approx -1.95$ , clearly underscoring the dominant role of the  $O(1/\omega^2)$  terms neglected in our approximation.

We now briefly touch upon the case where the coupling  $\kappa$  is also modulated in time, with the same periodicity as  $\gamma(\tau)$ . Then, we can still pursue the averaging avenue presented above. However, the end result will be somewhat different than the one obtained above. More specifically, equations (8) will still be valid but now with the effective couplings:

$$\kappa_{1\text{eff}} \equiv \frac{1}{T_0} \int_0^{T_0} \kappa(\tau) \exp[-2\Gamma(\tau)] d\tau, \quad \kappa_{2\text{eff}} \equiv \frac{1}{T_0} \int_0^{T_0} \kappa(\tau) \exp[2\Gamma(\tau)] d\tau. \quad (44)$$

These coefficients retrieve the earlier results of this and the previous dimer sections if  $\kappa(\tau) = \kappa$  i.e., for constant inter-node coupling. However, e.g. if  $\kappa(\tau) = e^{2\Gamma(\tau)}$ , then

$$\kappa_{1\text{eff}} = 1, \quad \kappa_{2\text{eff}} = \frac{1}{T_0} \int_0^{T_0} e^{4\Gamma(\tau)} d\tau. \quad (45)$$

We note that when  $\gamma_1(\tau) = \gamma_1 \cos(\tau)$ ,  $\kappa_{2\text{eff}} = I_0(4\gamma_1)$  where  $\gamma_1$  is a real constant. In this case, the eigenvalues of the effective linear problem would be  $\lambda_{1,2} = \pm \sqrt{\kappa_{1\text{eff}}\kappa_{2\text{eff}} - \gamma_0^2}$ . However, since for the case of a cosinusoidal drive  $I_0(4\gamma_1) > I_0(2\gamma_1)^2$ , this result suggests that it is possible through this additional modulation of the coupling strength to *further expand* the region of exact PT-symmetric phase in comparison to the case where only the gain/loss is modulated. While we do not explore this possibility further, we do note that it may be an especially relevant topic for further study.

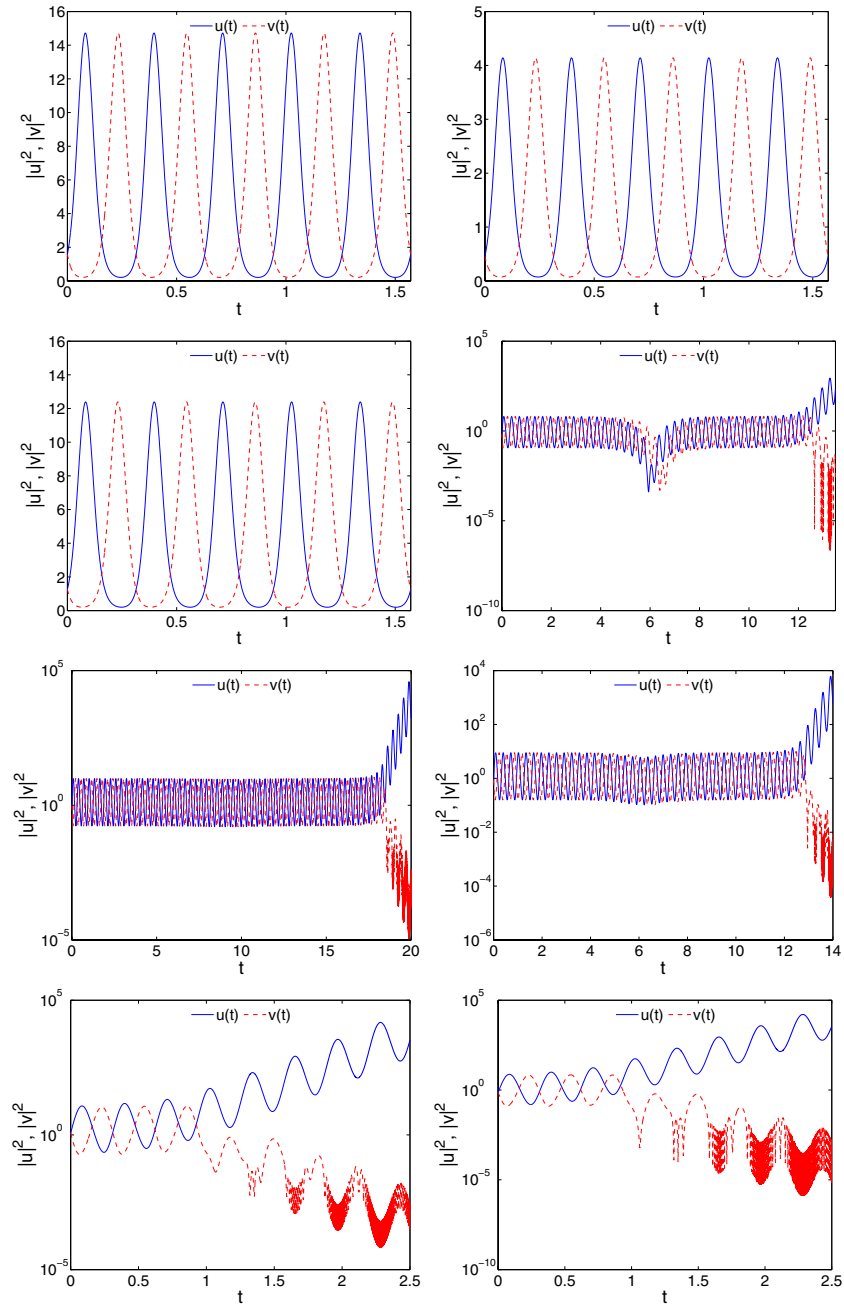


**Figure 2.** Dynamical evolution by means of full numerical simulations of former (at  $\gamma_0 = 0$ ) A solutions (left panels) and S solutions (right panels) for the modulated dimer in the case  $\kappa = 1$ ,  $E = 3$ ,  $\gamma_1 = 1$  and  $\omega = 20$ . Top panels correspond to a stable evolution at  $\gamma_0 = 1.5$  (which is already beyond the PT-phase transition critical point for  $\gamma_0$  in the case of  $\gamma_1 = 0$ ); panels of the second row show the stable (unstable) evolution for the A (S) solution at  $\gamma_0 = 2$ , whereas the third row displays the unstable evolution of solutions at  $\gamma_0 = 2.195$ . Finally, the bottom panels correspond to the evolution at  $\gamma_0 = 2.3$  (i.e. past the PT-symmetry breaking bifurcation) taking as initial condition the solution at  $\gamma_0 = 2.1$ .

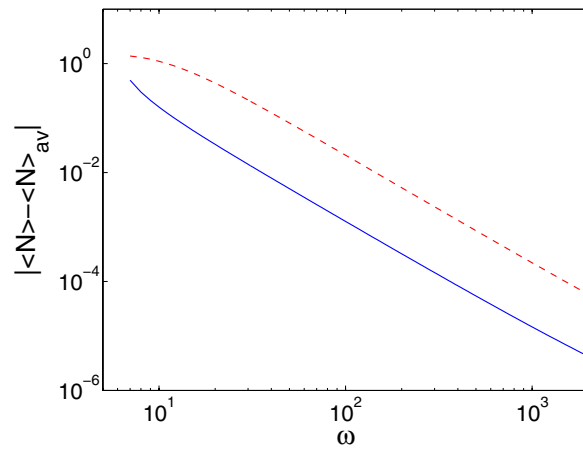


**Figure 3.** The figure represents the growth in the error of our averaging approximation for the quantity  $\langle N \rangle$  defined above. The blue solid line represents the S solution branch, while the dashed (red) line the A solution branch. The best fit of the slope for both branches is  $\approx -1.95$ .

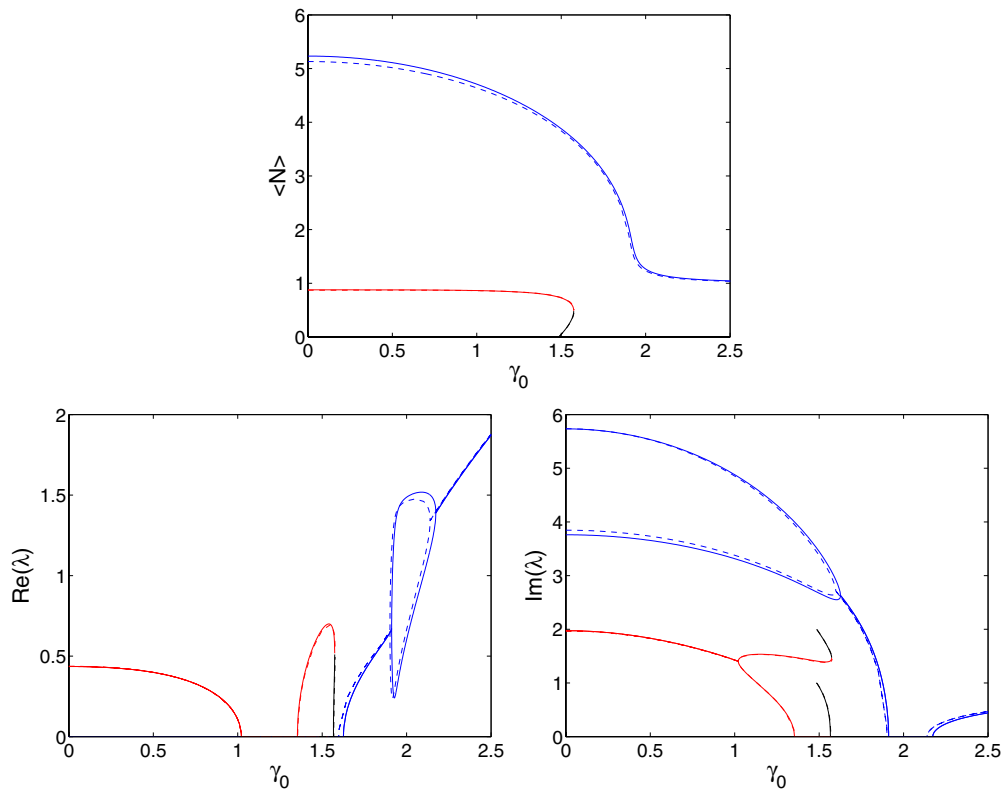


**Figure 4.** Averaged norm (top panel) and stability eigenvalues (bottom panels) for a trimer with  $\kappa = 1$ ,  $E = 1$  and  $\gamma_1 = 1$ ,  $\omega = 20$ . Solid (dashed) lines represent the values for the averaged (non-autonomous) system, whereas blue (red) line corresponds to the A (B) solution. The C solution is depicted as a black line.

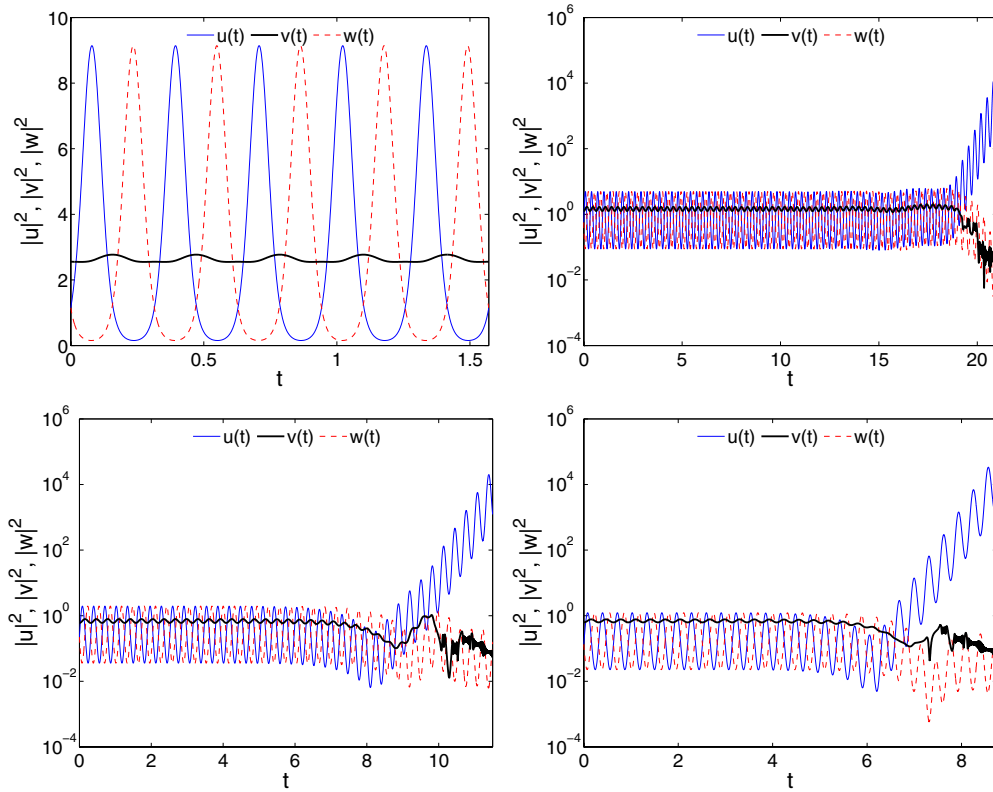


**Figure 5.** Dynamical evolution by means of full numerical simulations of A solutions for the modulated trimer in the case  $\kappa = 1$ ,  $E = 1$ ,  $\gamma_1 = 1$  and  $\omega = 20$ . The top left panel corresponds to a stable evolution at  $\gamma_0 = 0.5$ ; the top right panel shows the evolution of an oscillatorily unstable solution at  $\gamma_0 = 1.8$ ; the bottom left panel holds for an exponentially unstable solution at  $\gamma_0 = 2$ ; finally, the bottom right panel shows an oscillatorily unstable solution at  $\gamma_0 = 2.5$ .

#### 4.2. DNLS PT-symmetric trimer model

We now turn to the analysis of the trimer case, where  $\kappa' = \kappa I_0(\gamma_1)$  and  $g' = I_0(2\gamma_1)$ . In this case, the linear stability eigenvalues of the averaged system are unfortunately not available analytically and are, instead, found by numerical diagonalization. In the numerics, we have chosen the same parameters as in the dimer case except for  $E = 1$ .

In agreement with what has been reported earlier for Schrödinger trimers without time-modulation [18, 45], we have identified three distinct stationary solutions, which we will denote hereafter as A, B and C. Solutions A and B exist at  $\gamma_0 = 0$  and are characterized, at this limit, in the first case by a phase difference between the sites of  $\pi$ , so that  $u(t) = w(t) \neq v(t)$ ; in the second case,  $v(t) = 0$  and there is a phase difference of  $\pi$  between the first and third node, i.e.  $u(t) = -w(t)$ . The third branch of solutions, namely C, exists for  $\gamma_0 \geq \sqrt{2\kappa^2 I_0^2(\gamma_1) - E^2} \approx 1.4852$ . Interestingly, there is a qualitative difference in the bifurcation diagram (an imperfect pitchfork, which leads to an isolated branch and a saddle-node bifurcation) between the case examined in [18, 45] and the one considered herein. In the former, the solutions A and B terminate through a saddle-node and the C solution is the isolated branch of the imperfect pitchfork. However, in our present system, it is the B and C solutions which cease to exist at the fold point of  $\gamma_0 = 1.5741$ , whereas the isolated branch

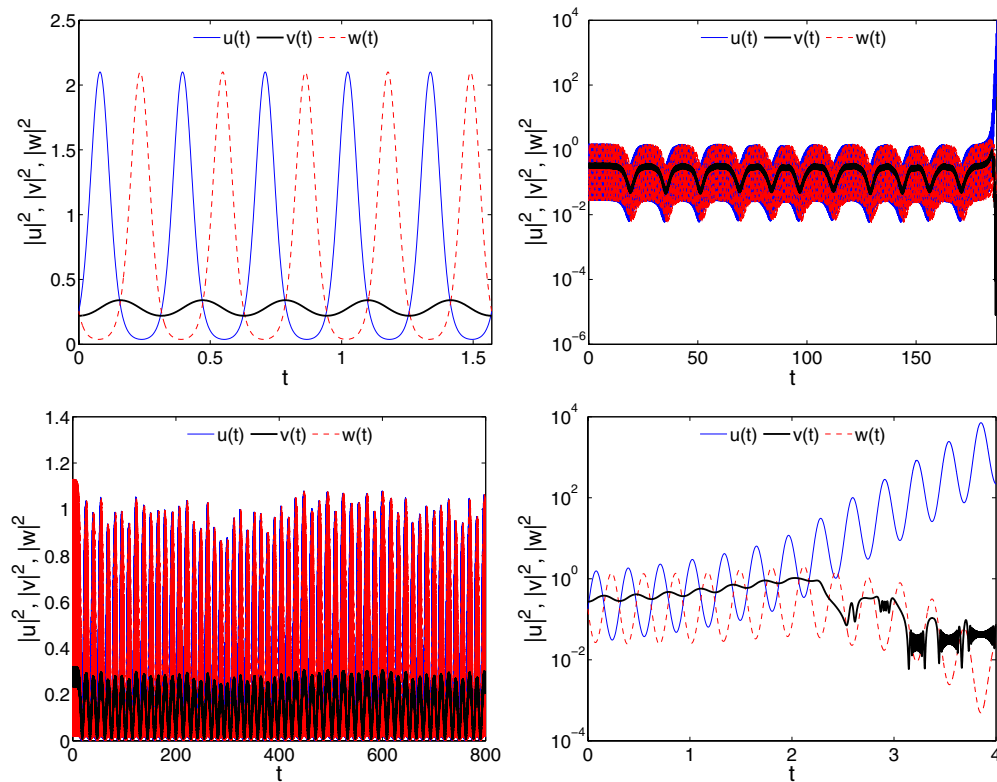


**Figure 6.** Dynamical evolution by means of full numerical simulations of B solutions for the modulated trimer in the case  $\kappa = 1, E = 1, \gamma_1 = 1$  and  $\omega = 20$ . The top left panel corresponds to a stable evolution at  $\gamma_0 = 1.2$ ; the top right panel shows the evolution of an oscillatorily unstable solution at  $\gamma_0 = 0.5$ ; the bottom left panel represents an exponentially unstable solution at  $\gamma_0 = 1.57$ ; finally, the bottom right panel shows the evolution at  $\gamma_0 = 1.7$  (i.e. past the collision with branch C) using as initial condition the solution at  $\gamma_0 = 1.5$ .

is now the A one. These results are predicted by the averaged model and corroborated by the numerical analysis of the modulated system and the corresponding numerically exact (up to the prescribed tolerance of  $10^{-12}$ ) time-periodic solutions. Nevertheless, we have checked that for different values of  $\kappa'$  and  $g'$ , various features of the bifurcation diagram may change. These include the above mentioned possibility of A and B colliding rather than B and C, as well as even the possibility of a fourth (D) branch of solutions emerging in the nonlinear system. The latter case is non-generic, and the bifurcation scheme strongly depends on  $\kappa'$  and  $g'$ ; for instance, at  $\kappa' = 0.1$  and  $g' = I_0(2\gamma_1)$  the four branches exist at the Hamiltonian limit (with C and D branches corresponding to in phase solutions) and bifurcate branch A with C and B with D through saddle-nodes when  $\gamma_0$  is increased.

Figure 4 shows both the averaged norm and the stability eigenvalues (imaginary and real parts), together with the predicted values by the averaged equations. Obviously, the prediction of the averaged system is excellent for the B and C solutions, with a small discrepancy arising only for the A solution. We observe that the A solution is stable for small  $\gamma_0$ , becoming unstable through a Hamiltonian Hopf bifurcation [48]<sup>8</sup> at  $\gamma_0 = 1.5983$  (1.6261 in the averaged system).

<sup>8</sup> It is interesting to note here that despite the fact that the system is no longer Hamiltonian, the bifurcation arising has all the characteristics of Hamiltonian Hopf including the collision of two eigenvalues and the formation of a quartet.



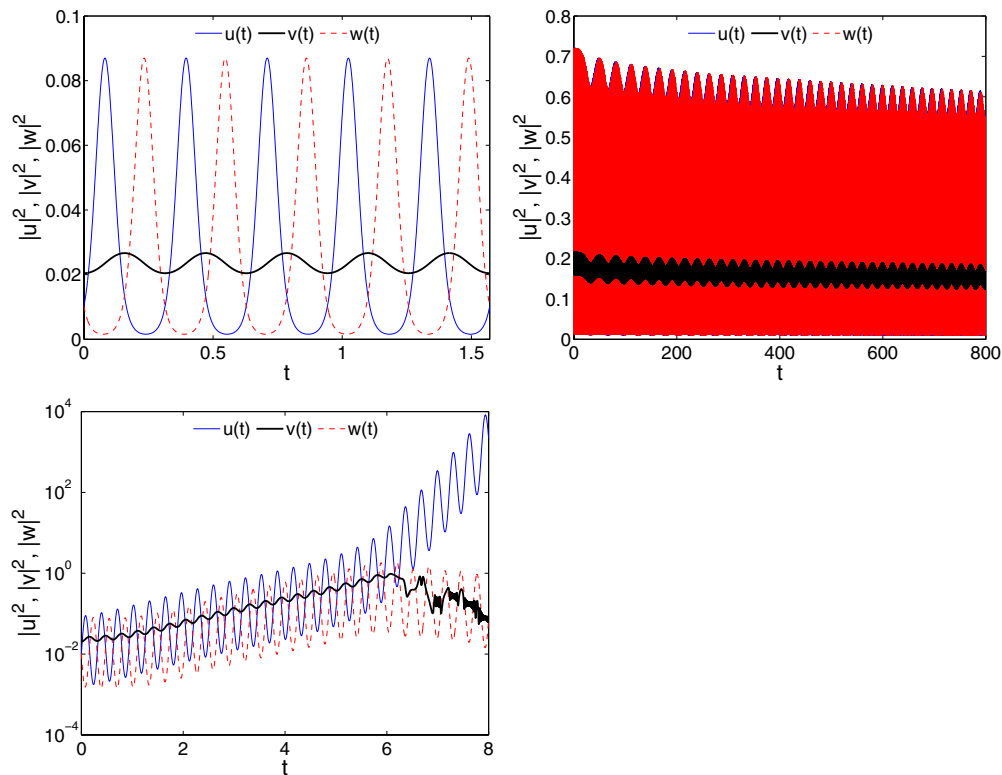


**Figure 7.** Dynamical evolution by means of full numerical simulations of C solutions for the modulated trimer in the case  $\kappa_0 = 1$ ,  $E = 1$ ,  $\gamma_1 = 1$  and  $\omega = 20$ . The top left panel corresponds to a stable evolution at  $\gamma_0 = 1.5$ ; the top right panel shows the evolution of an exponentially unstable solution at  $\gamma_0 = 1.57$ ; the bottom left panel corresponds to the case of  $\gamma_0 = 1.7$  (i.e. past the saddle-node bifurcation with branch B) using as initial condition the solution at  $\gamma_0 = 1.5$ .

The imaginary part of that quadruplet of eigenvalues becomes zero (i.e., the instability becomes exponential) in the range  $\gamma_0 \in [1.9014, 2.1391]$  ( $[1.9116, 2.1731]$  for the averaged system); the instability becomes again oscillatory above this range. The B solution is oscillatorily unstable for small  $\gamma_0$ , becoming stable via inverse Hopf bifurcation at  $\gamma_0 = 1.0216$  (1.0214 in the averaged case). The solution becomes exponentially unstable for  $\gamma \geq 1.3552$  (1.3534, respectively for the effective autonomous equation), finally colliding with the C solution and disappearing in the relevant saddle-node bifurcation at  $\gamma_0 = 1.5764$  (1.5741 in the averaged system) as explained above. The C solution, which does not exist for  $\gamma_0 < 1.4869$  (1.4852 in the averaged system), is stable up to  $\gamma_0 = 1.5687$  (1.5667, respectively for the non-autonomous case), beyond which it experiences exponential growth due to a real eigenvalue. It is clear from the above comparisons that there is an excellent agreement between the predictions of the original system and its effective, averaged description.

Figures 5–7 show the dynamical evolution of A, B and C solutions, respectively. In the case of A solutions, we can observe their dynamical stability for sufficiently low values of  $\gamma_0$  (top left panel). As  $\gamma_0$  is increased, initially an oscillatory (top right) and subsequently an exponential (bottom left) instability arises. In the dynamical evolutions, the fate of the

We note that it would be especially interesting to consider the question of the potential existence of an analogous notion to the Krein signature for these PT-symmetric systems that could predict such potential Hopf bifurcations and quartet formations.

solutions appears to be similar, with the gain site ultimately growing, while the other two sites are eventually observed to decay in amplitude. Nevertheless, the exponential instability appears to manifest itself faster, in consonance with our eigenvalue findings above. As we progress to higher  $\gamma_0$ , an oscillatory instability arises again, as shown in the bottom right panel but this time with a high growth rate and a rapid destabilization accordingly.

The dynamics of the B branch is, arguably, somewhat more complex in figure 6. While a stable evolution for  $\gamma_0 = 1.2$  is shown in the top left panel, for smaller values of  $\gamma_0$  (such as  $\gamma_0 = 0.5$  of the top right panel), an oscillatory instability is present and appears to lead to indefinite growth of the gain site, while the other two sites decay in amplitude. Perhaps most intriguing is the case of  $\gamma_0 = 1.57$  of the bottom left panel of the figure. Here, the dynamics does not appear to diverge, but rather seems to revert to a quasi-periodic motion, yielding a bounded dynamical result. On the other hand, in the bottom right case of  $\gamma_0 = 1.7$ , past the critical point of the bifurcation with branch C, the dynamics is led to indefinite growth (again with the gain site growing, while the other two are decaying in amplitude).

Lastly, we consider different dynamical examples from within the narrow interval of existence of branch C in figure 7. In the top left panel case of  $\gamma_0 = 1.5$ , the stable evolution of this branch is depicted. The exponential instability of the branch in the top right panel for  $\gamma_0 = 1.57$  appears, similarly to branch B, to lead not to indefinite growth but rather to quasi-periodic oscillation and a bounded dynamical evolution. On the contrary, for values of  $\gamma_0$  past the saddle-node bifurcation with branch B (but similarly to the dynamics of branch B for such values of  $\gamma_0$ ), we observe (cf bottom left panel) indefinite growth in the dynamics for  $\gamma_0 = 1.7$ .

## 5. Conclusions and future challenges

In the present work, we have explored the potential of PT-symmetric oligomer system (a dimer and a trimer more concretely, although generalizations to a higher number of sites are directly possible) to have its gain/loss pattern periodically modulated in time. Although this possibility may be somewhat more limited in optical systems, it should in principle be possible in electric circuit settings. As we argued, additionally, this kind of possibility may bear *significant* advantages including most notably the *expansion* of the exact PT-symmetric phase region. The latter threshold at the linear level now becomes  $\gamma_0 I_0(2\gamma_1)$  or  $\sqrt{2}\gamma_0 I_0(\gamma_1)$ , for the dimer and trimer, respectively, for a modulated gain/loss coefficient with mean value  $\gamma_0$  and a periodic modulation of amplitude  $\gamma_1$  and frequency  $\omega$ . In addition to this expansion, we were able through our averaging procedure to reduce the non-autonomous full problem to an effective time-independent (averaged) one, for which a lot of information (especially so for the dimer case) can be obtained analytically, including the existence and stability of the relevant solutions. The results of the averaged equation approximation were generally found, in the appropriate regime, to be in *excellent* agreement with those of the full, time-dependent problem and its periodic solutions and their Floquet exponents. This was the case both for the (former) symmetric and antisymmetric branches of the dimer and the collision leading to their termination, but also for the branches identified in the trimer, representing an apparent example of an imperfect pitchfork bifurcation.

One can envision many interesting and relevant extensions of the present work. One such would be to consider the case where the PT-symmetry ‘management’ could be applied to a full lattice or to a chain of dimers, as in the work of [20]. There, it would be quite relevant to explore the impact of the modulation to the solitary waves and localized solutions of the lattice. Another possibility is to consider generalizations of this ‘linear’ PT-symmetry management towards a nonlinear variant thereof. More specifically, in the spirit of [37–40],

a PT-symmetric gain/loss term could be applied to the nonlinear part of the dimer/trimer or lattice. Then, one can envision a generalization of the notion of nonlinearity management and of the corresponding averaging (see e.g. [49, 50]), in order to formulate novel effective lattice media as a result of the averaging. Such possibilities are currently under investigation and will be reported in future publications.

## Acknowledgments

PGK gratefully acknowledges support from the US National Science Foundation (grant DMS-0806762 and CMMI-1000337), the Alexander von Humboldt Foundation and the US AFOSR under grant FA9550-12-1-0332. PGK, RLH and NW gratefully acknowledge a productive visit to the IMA at the University of Minnesota. JC acknowledges financial support from the MICINN project FIS2008-04848. The work of DJF was partially supported by the Special Account for Research Grants of the University of Athens.

## References

- [1] Bender C M and Boettcher S 1998 *Phys. Rev. Lett.* **80** 5243  
Bender C M, Boettcher S and Meisinger P N 1999 *J. Math. Phys.* **40** 2201
- [2] Ruschhaupt A, Delgado F and Muga J G 2005 *J. Phys. A: Math. Gen.* **38** L171
- [3] Musslimani Z H, Makris K G, El-Ganainy R and Christodoulides D N 2008 *Phys. Rev. Lett.* **100** 030402  
Makris K G, El-Ganainy R, Christodoulides D N and Musslimani Z H 2010 *Phys. Rev. A* **81** 063807
- [4] Ramezani H, Kottos T, El-Ganainy R and Christodoulides D N 2010 *Phys. Rev. A* **82** 043803
- [5] Kulishov M and Kress B 2012 *Opt. Express* **20** 29319
- [6] Rüter C E, Makris K G, El-Ganainy R, Christodoulides D N, Segev M and Kip D 2010 *Nature Phys.* **6** 192
- [7] Guo A, Salamo G J, Duchesne D, Morandotti R, Volatier-Ravat M, Aimez V, Siviloglou G A and Christodoulides D N 2009 *Phys. Rev. Lett.* **103** 093902
- [8] Schindler J, Li A, Zheng M C, Ellis F M and Kottos T 2011 *Phys. Rev. A* **84** 040101
- [9] Schindler J, Lin Z, Lee J M, Ramezani Hamidreza, Ellis F M and Kottos T 2012 *J. Phys. A: Math. Theor.* **45** 444029
- [10] Bender C M, Berntson B, Parker D and Samuel E 2013 *Am. J. Phys.* **81** 173
- [11] Peng B, Özdemir S K, Lei F, Monifi F, Gianfreda M, Long G L, Fan S, Nori F, Bender C M and Yang L 2013 arXiv:1308.4564
- [12] Ramezani H, Kottos T, El-Ganainy R and Christodoulides D N 2010 *Phys. Rev. A* **82** 043803
- [13] Sukhorukov A A, Xu Z and Kivshar Yu S 2010 *Phys. Rev. A* **82** 043818
- [14] Zheng M C, Christodoulides D N, Fleischmann R and Kottos T 2010 *Phys. Rev. A* **82** 010103
- [15] Graefe E M, Korsch H J and Niederle A E 2008 *Phys. Rev. Lett.* **101** 150408
- [16] Graefe E M, Korsch H J and Niederle A E 2010 *Phys. Rev. A* **82** 013629
- [17] Lin Z, Ramezani H, Eichelkraut T, Kottos T, Cao H and Christodoulides D N 2011 *Phys. Rev. Lett.* **106** 213901
- [18] Li K and Kevrekidis P G 2011 *Phys. Rev. E* **83** 066608
- [19] Dmitriev S V, Suchkov S V, Sukhorukov A A and Kivshar Yu S 2011 *Phys. Rev. A* **84** 013833
- [20] Suchkov S V, Malomed B A, Dmitriev S V and Kivshar Yu S 2011 *Phys. Rev. E* **84** 046609
- [21] Abdullaev F Kh, Konotop V V, Ögren M and Sørensen M P 2011 *Opt. Lett.* **36** 4566
- [22] Alexeeva N V, Barashenkov I V, Sukhorukov A A and Kivshar Yu S 2012 *Phys. Rev. A* **85** 063837
- [23] Sukhorukov A A, Dmitriev S V and Kivshar Yu S 2012 *Opt. Lett.* **37** 2148
- [24] Cartarius H and Wunner G 2012 *Phys. Rev. A* **86** 013612  
Cartarius H and Wunner G 2012 *J. Phys. A: Math. Theor.* **45** 444008
- [25] Graefe E-M 2012 *J. Phys. A: Math. Theor.* **45** 444015
- [26] Rodrigues A S, Li K, Achilleos V, Kevrekidis P G, Frantzeskakis D J and Bender C M 2013 *Rom. Rep. Phys.* **65** 5
- [27] Barashenkov I V, Suchkov S V, Sukhorukov A A, Dmitriev S V and Kivshar Yu S 2012 *Phys. Rev. A* **86** 053809
- [28] Barashenkov I V, Baker L and Alexeeva N V 2013 *Phys. Rev. A* **87** 033819
- [29] Zezyulin D A and Konotop V V 2012 *Phys. Rev. Lett.* **108** 213906
- [30] Leykam D, Konotop V V and Desyatnikov A S 2013 *Opt. Lett.* **38** 371
- [31] Li K, Zezyulin D A, Konotop V V and Kevrekidis P G 2013 *Phys. Rev. A* **87** 033812

- [32] Achilleos V, Kevrekidis P G, Frantzeskakis D J and Carretero-González R 2012 *Phys. Rev. A* **86** 013808  
Achilleos V, Kevrekidis P G, Frantzeskakis D J and Carretero-González R 2012 arXiv:1202.1310
- [33] Bludov Yu V, Konotop V V and Malomed B A 2013 *Phys. Rev. A* **87** 013816
- [34] Li K, Kevrekidis P G, Malomed B A and Günther U 2012 *J. Phys. A: Math. Theor.* **44** 444021
- [35] Kevrekidis P G, Pelinovsky D E and Tyugin D Y 2013 *SIAM J. Appl. Dyn. Syst.* **12** 1210  
Kevrekidis P G, Pelinovsky D E and Tyugin D Y 2013 *J. Phys. A: Math. Theor.* **46** 365201
- [36] Pickton J and Susanto H 2013 arXiv:1307.2788
- [37] Miroshnichenko A E, Malomed B A and Kivshar Yu S 2011 *Phys. Rev. A* **84** 012123
- [38] Abdullaev F Kh, Kartashov Y V, Konotop V V and Zezyulin D A 2011 *Phys. Rev. A* **83** 041805
- [39] Zezyulin D A, Kartashov Y V and Konotop V V 2011 *Europhys. Lett.* **96** 64003
- [40] Duanmu M, Li K, Horne R L, Kevrekidis P G and Whitaker N 2013 *Phil. Trans. R. Soc. A* **371** 20120171
- [41] Malomed B A 2006 *Soliton Management in Periodic Systems* (Berlin: Springer)
- [42] Turitsyn S K, Bale B G and Fedoruk M P 2012 *Phys. Rep.* **521** 135
- [43] Driben R and Malomed B A 2011 *Opt. Lett.* **36** 4323
- [44] Driben R and Malomed B A 2011 *Europhys. Lett.* **96** 51001
- [45] Li K, Kevrekidis P G, Frantzeskakis D J, Rüter C E and Kip D 2013 arXiv:1306.2255
- [46] Flach S and Gorbach A V 2008 *Phys. Rep.* **467** 1  
Palmero F, English L Q, Cuevas J, Carretero-González R and Kevrekidis P G 2011 *Phys. Rev. E* **84** 026605  
Cretegny T and Aubry S 1997 *Phys. Rev. B* **55** R11929  
Gómez-Gardeñes J, Floría L M, Peyrard M and Bishop A R 2004 *Chaos* **14** 1130  
Melvin T R O, Champneys A R, Kevrekidis P G and Cuevas J 2008 *Physica D* **237** 551–67
- [47] Cuevas J, Kevrekidis P G, Saxena A and Khare A 2013 *Phys. Rev. A* **88** 032108
- [48] see, e.g., MacKay R S 1987 *Hamiltonian Dynamical Systems* ed R S MacKay and J Meiss (Bristol: Hilger)  
p 137
- [49] Pelinovsky D E, Kevrekidis P G and Frantzeskakis D J 2003 *Phys. Rev. Lett.* **91** 240201  
Pelinovsky D E, Kevrekidis P G, Frantzeskakis D J and Zharnitsky V 2004 *Phys. Rev. E* **70** 047604  
Zharnitsky V and Pelinovsky D E 2005 *Chaos* **15** 037105  
Kevrekidis P G, Pelinovsky D E and Stefanov A 2006 *J. Phys. A: Math. Gen.* **39** 479
- [50] Abdullaev F Kh, Tsoy E N and Malomed B A 2013 *Phys. Rev. A* **68** 053606  
Abdullaev F Kh, Kevrekidis P G and Salerno M 2010 *Phys. Rev. Lett.* **105** 113901